View Article Online / Journal Homepage / Table of Contents for this issue
Dynamic Article Links

ChemComm

Cite this: *Chem. Commun.*, 2012, **48**, 3686–3699

www.rsc.org/chemcomm

FEATURE ARTICLE

Graphene quantum dots: emergent nanolights for bioimaging, sensors, catalysis and photovoltaic devices

Jianhua Shen, Yihua Zhu,* Xiaoling Yang and Chunzhong Li*

Received 6th January 2012, Accepted 17th February 2012
DOI: 10.1039/c2cc00110a

Similar to the popular older cousins, luminescent carbon dots (C-dots), graphene quantum dots or graphene quantum discs (GQDs) have generated enormous excitement because of their superiority in chemical inertness, biocompatibility and low toxicity. Besides, GQDs, consisting of a single atomic layer of nano-sized graphite, have the excellent performances of graphene, such as high surface area, large diameter and better surface grafting using π–π conjugation and surface groups. Because of the structure of graphene, GQDs have some other special physical properties. Therefore, studies on GQDs in aspects of chemistry, physical, materials, biology and interdisciplinary science have been in full flow in the past decade. In this Feature Article, recent developments in preparation of GQDs are discussed, focusing on the main two approaches (top-down and bottom-down). Emphasis is given to their future and potential development in bioimaging, electrochemical biosensors and catalysis, and specifically in photovoltaic devices that can solve increasingly serious energy problems.

1. Introduction

Fluorescent materials produce visible or invisible light as a result of incident light of a different wavelength. The effect ceases as soon as the source of excitement is removed. Semiconductor based quantum dots (QDs) have proven themselves as powerful inorganic fluorescent probes, especially for long term resistance to photobleaching.[1] However, size-tunable properties have become a hallmark of quantum dots and related nanostructures.[2] Recent advances have led to the development of dendrimer-encapsulated quantum dots,[3,4] synthesis of quantum dots in mesopores,[5,6] core–shell colloidal nanostructured quantum dots,[7,8] and mixed semiconductor dots,[9,10] and so on.[11] However, compared to conventional semiconductor quantum dots, carbon dots (C-dots) are superior in terms of chemical inertness, low cytotoxicity and excellent biocompatibility.[12,13] C-dots constitute a fascinating class of recently discovered nanocarbons that comprise discrete, quasi-spherical nanoparticles with sizes below 10 nm.[13–28] They possess several favorable attributes, such as resistance to photobleaching, size- and wavelength-dependent luminescence emission, ease of production and bioconjugation,

Key Laboratory for Ultrafine Materials of Ministry of Education, School of Materials Science and Engineering, East China University of Science and Technology, Shanghai 200237, China.
E-mail: yhzhu@ecust.edu.cn, czli@ecust.edu.cn;
Fax: +86 21 6425 0624; Tel: +86 21 6425 2022

Jianhua Shen

Jianhua Shen obtained his BS degree from School of Materials Science and Engineering, East China University of Science and Technology (ECUST) in 2009. He is currently a PhD student in Key Laboratory for Ultrafine Materials of Ministry of Education, ECUST, with Professor Yihua Zhu, focusing on graphene quantum dots and multifunctional magnetic nanocomposites.

Yihua Zhu

Yihua Zhu received his BS degree from Nanjing University and MS and PhD degrees from East China University of Science and Technology (ECUST). Currently he is a full professor in Key Laboratory for Ultrafine Materials of Ministry of Education, ECUST. His research interests include porous materials and nano-structured materials and related functional applications, especially for biosensors, drug delivery, catalysis and clean energy.

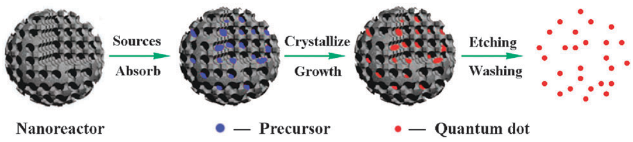

Fig. 1 Schematic diagram of confined reaction in nanoreactors to prepare quantum dots.

use of cheap and abundant raw materials.[13] Advances in this area are appearing frequently, with a number of significant breakthroughs taking place within the last couple of years. A variety of methods have been developed to prepare C-dots. They can be prepared by laser ablation of graphite,[14,15] electrochemical oxidation of graphite,[16] supported routes,[17] electrochemical soaking of carbon nanotubes,[18] thermal oxidation of suitable molecular precursors,[19,20] from the combustion soot of candles[21] or natural gas,[22] proton-beam irradiation of nanodiamonds,[23] microwave synthesis,[24] and so on.[25–27] Very recently, Zhu *et al.* have reported a simple bottom-up synthesis method for C-dots by using a mesoporous silica microspheres template.[28] They proposed the concept of confined reaction in nanoreactors to prepare nanoparticles (Fig. 1).

In addition to the above properties, graphene quantum dots or graphene quantum discs (GQDs), as a kind of C-dots, have the excellent performance of graphene. Over the past few decades, graphene, a single layer of carbon atoms in a honeycomb structure, has generated enormous excitement due to its large surface area,[29,30] high carrier transport mobility,[31,32] superior mechanical flexibility[33] and excellent thermal/chemical stability.[34–37] With bulk graphene having a zero bandgap, in principle the bandgap of graphenes can be tuned from 0 eV to that of benzene by varying their sizes.[38–40] To facilitate the application of graphene in nanodevices and effectively tune the bandgap of graphenes, a promising approach is to convert the 2D graphene sheets into 0D GQDs. These GQDs exhibit new phenomena due to quantum confinement and edge effects, which are similar to C-dots. However, the disadvantage is that C-dots possess size effects, and quasi-spherical nanoparticles with sizes below 10 nm.[13] Therefore, GQDs and their chemical derivatives have received more attention, as their diameters are mainly distributed in a larger range (3–20 nm).[13,40]

Typically, GQDs contain carboxylic acid moieties at the edge, which is similar to graphene, thus imparting them with excellent water solubility and suitability for subsequent functionalization with various organic, polymeric, inorganic or biological species (Fig. 2). In addition, GQDs have some excellent characteristics, such as high surface area, larger diameter, better surface grafting using the π–π conjugated network or surface groups and other special physical properties due to the structure of graphene. As a consequence of their simple structure, as well as health concerns and biological hazards of QDs, GQDs are at the center of significant research efforts to develop low-toxicity, eco-friendly alternatives that have the desirable performance characteristics of QDs. It is our aim that the development of this knowledge will offer valuable insights; moreover, we hope to inspire research into the origins of the unique properties of emerging novel fluorescent materials such as BN quantum dots, Si quantum dots, nanodiamonds, *etc.*, and to encourage their exploration in electrochemical biosensors, bioimaging, drug delivery and energy conversion.

2. Synthetic methods

Approaches for synthesizing GQDs with tunable size can be generally classified into two main groups: top-down and bottom-up methods (Fig. 3). Top-down approaches refer to the cutting of graphene sheets into GQDs, the method consists of chemical ablation, electrochemical oxidation, and oxygen plasma treatment, where GQDs are formed or "broken off" from larger graphene sheets. Bottom-up methods involve the synthesis of graphene moieties containing a certain number of conjugated carbon atoms, the approaches consist, for example, of the cage-opening of fullerene, or solution chemistry methods during which the GQDs are formed from molecular precursors. Typically, these GQDs have surfaces rich in carboxylic acid functionalities which can be used to bind surface-passivation reagents.

Xiaoling Yang

Xiaoling Yang received her BS, MS and PhD degrees from East China University of Science and Technology (ECUST). Currently she is an associate professor in Key Laboratory for Ultrafine Materials of Ministry of Education, ECUST. Her current research interests include materials science and nano-technology with a particular focus on nano-composites for catalysis and medical application.

Chunzhong Li

Chunzhong Li received his BS, MS and PhD degrees from East China University of Science and Technology in 1989, 1992, and 1997, respectively. He became a full professor of school of materials science and engineering in 1998, and now he is the director of Key Laboratory for Ultrafine Materials of the Ministry of Education at East China University of Science and Technology. In 2009, he became the winner of the National Science Fund for Distinguished Young Scholars. His research interests include functionalization and fabrication of nanomaterials and for applications in catalysis, clean energy and biomedical areas.

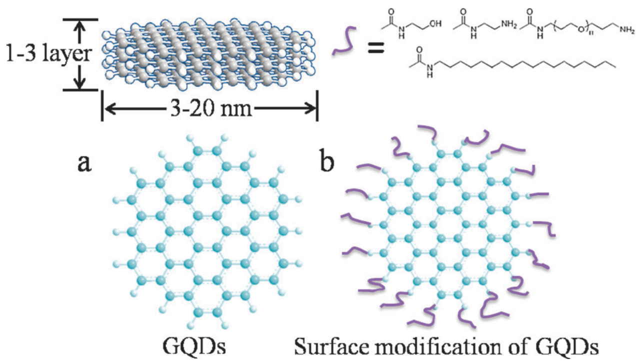

Fig. 2 (a) Depiction of GQDs and (b) structural models after functionalization with surface-passivation reagents.

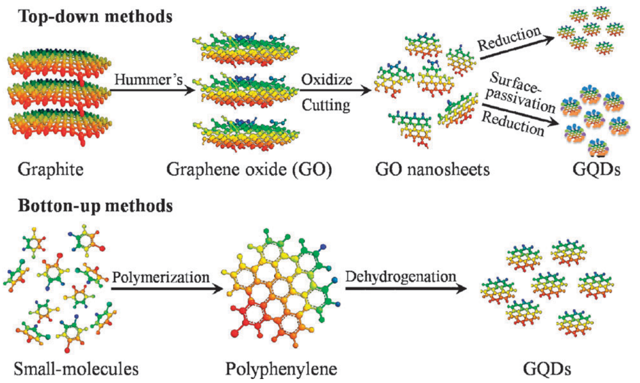

Fig. 3 Schematic diagram of the top-down and bottom-up methods for synthesizing GQDs.

2.1. Top-down approaches

2.1.1. Chemical ablation from graphene. In 2008, Dai and co-workers reported intrinsic luminescence from predominantly single-layer nanographene oxide sheets in both the visible and NIR regions.[41] Pan *et al.* developed a hydrothermal route to cutting graphene sheets into GQDs, exhibiting blue luminescence.[42] Briefly, the large graphene oxide sheets were cut into small sheets by controlled oxidation in a mixture of sulfuric acid and nitric acid under mild ultrasonication. The oxidized small graphene sheets were then reduced under hydrothermal conditions in a Teflon lined autoclave at elevated temperature. The obtained GQDs had an average diameter of 9.6 nm (Fig. 4a) consisting of 1–3 layers of graphene, and exhibited a quantum yield of 6.9% using quinine sulfate as a reference. Shen *et al.* prepared GQDs surface-passivated by polyethylene glycol (GQDs-PEG) by a one-pot hydrothermal reaction, using small graphene oxide (GO) sheets and polyethylene glycol (PEG) as starting materials.[40] The collected GQDs-PEG were nearly monodisperse with a uniform diameter of *ca.* 5–25 nm (Fig. 4b). By comparing the GQDs-PEG and the GQDs, the prepared GQDs-PEG show excellent luminescence properties, the PL quantum yield of the GQDs-PEG with 360 nm emission was about 28.0% using rhodamine B as a reference. Zhu *et al.* synthesized smaller GQDs with strong green photoluminescence by a one-step solvothermal method.[43] The average diameters of GQDs were 5.3 nm, and their average height was 1.2 nm, from which it was concluded that most of the GQDs were single or bi-layered (Fig. 4c).

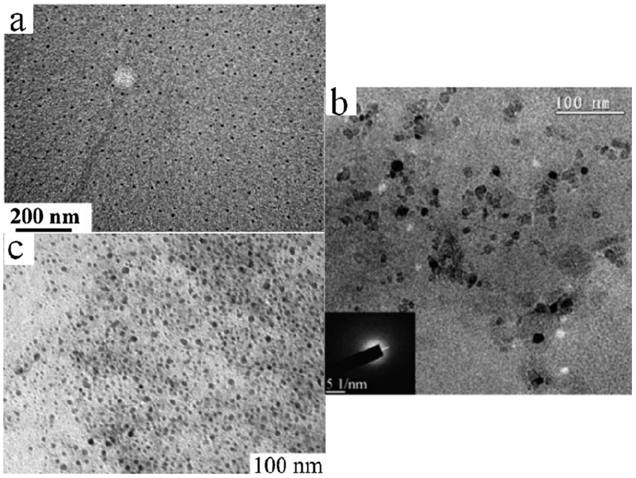

Fig. 4 TEM images of (a) blue-luminescent GQDs produced by hydrothermally cutting graphene sheets, (b) GQDs-PEG obtained by one-pot hydrothermal reaction and (c) green-luminescent GQDs obtained by one-step solvothermal method. Reprinted with permission from refs. 42, 40 and 43. Copyright 2010 and 2011.

In addition to hydrothermal or solvothermal methods, GQDs were also prepared by traditional hydrazine hydrate reduction of oxidized small graphene sheets. Zhu and co-workers reported GQDs prepared by hydrazine hydrate reduction of GO with their surface passivated by PEG.[44] First, GO was further oxidised by HNO_3, and cut into small GO sheets. Then, the GQD precursor was treated with an oligomeric PEG diamine (PEG_{1500N}) as a surface passivation agent (Fig. 5). The precursor was finally reduced by hydrazine hydration to fabricate GQDs. Strong blue PL was clearly shown under 365 nm radiation and green fluorescence was observed under a 980 nm laser. The PL quantum yield measured using rhodamine B as a reference is 7.4%. Prior to this work, Chhowalla and co-workers had reported the PL intensity of a GO thin film was changed after each incremental hydrazine-vapor exposure (from 20 s up to 60 min).[45] It is immediately clear that in contrast to the broad absorption features, a relatively narrow PL peak centered around 390 nm is observed. One possible origin of the blue PL is the radiative recombination of e–h pairs generated within localized states. The energy gap between the π and π^* states generally depends on the size of sp^2 clusters or conjugation length.[46] While the PL intensity was weak for as-deposited GO films, short exposure to hydrazine vapor results in a dramatic increase in

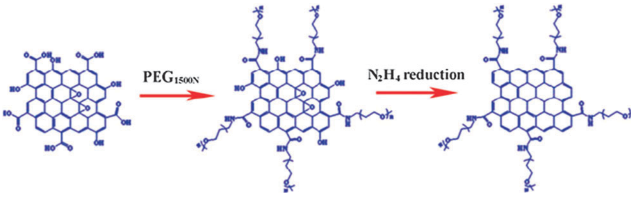

Fig. 5 Representation of GQDs containing an oligomeric PEG diamino-surface passivating agent. Reprinted with permission from ref. 44. Copyright 2011.

the PL intensities. Interestingly, this trend was reversed after >3 min exposure to hydrazine vapor. Longer exposure leaded to eventual quenching of the PL signal.

2.1.2. Electrochemical synthesis. Zhou *et al.* first demonstrated the electrochemical synthesis of C-dots from multiwalled carbon nanotubes (MWCNTs) formed from scrolled graphene layers on carbon paper by CVD.[16] Another research group produced C-dots electrochemically by oxidizing a graphitic column electrode at 3 V (*vs.* saturated calomel electrode) with a Pt wire counter-electrode in 0.1 M NaH_2PO_4 aqueous solution.[47] Chi and co-workers also produced C-dots electrochemically from a graphite rod working electrode, a Pt mesh counter-electrode, and a Ag/AgCl reference electrode assembly immersed in pH 7.0 phosphate buffer solution.[48] Although graphite was used as a raw material, spherical dots were produced with sizes of about 2 to 20 nm, which were not considered as GQDs.[13] Loh and co-workers generated fluorescent carbon nanoribbons, nanoparticles and graphene from graphite electrode by ionic liquid (IL) assisted electrochemical exfoliation using the water-soluble IL 1-butyl-3-methylimidazolium tetrafluoroborate [bmim][BF_4] containing up to 90 wt% water as the electrolyte.[49] The mechanism of the exfoliation was due to a complex interplay of anodic oxidation of water and anionic intercalation from the ionic liquid. Using ILs with high water content ($>10\%$ water) as the electrolyte, water-soluble, oxidized carbon nanomaterials were generated. In the case of electrolyte using concentrated ILs ($<10\%$ water), IL-functionalized carbon nanomaterials were generated instead. Carbon nanoribbons, which have a similar structure to GQDs, could be produced directly from graphite by the concerted action of anionic intercalation and oxidative cleavage (Fig. 6).

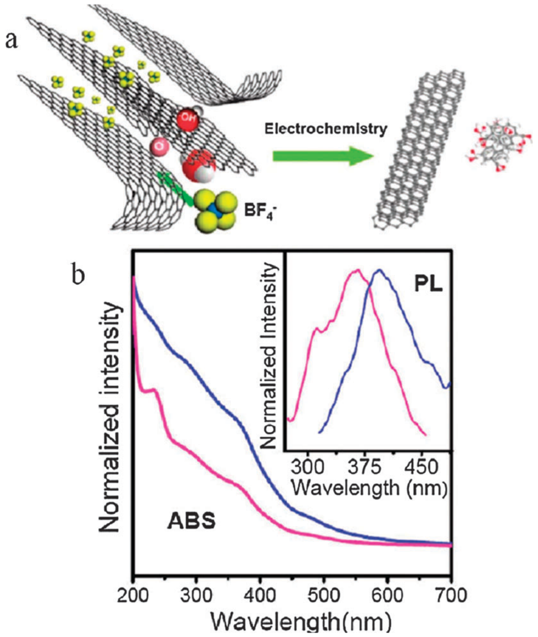

Fig. 6 (a) Illustration of the exfoliation process showing the attack of the graphite edge planes by hydroxyl and oxygen radicals, which facilitate the intercalation of BF_4^- anion. The dissolution of hydroxylated carbon nanoparticles gives rise to fluorescent carbon nanoparticles. Oxidative cleavage of the expanded graphite produces graphene nanoribbons. (b) UV-vis absorption and fluorescence spectra (inset figure) obtained for 8–10 nm carbon nanoparticles (red curve) and carbon nanoribbons (blue curve). The emission spectrum was obtained using 260 nm excitation. Reprinted with permission from ref. 49. Copyright 2009.

Later, Li *et al.* reported an electrochemical means of synthesizing green-luminescent functional GQDs with a uniform size of 3–5 nm (Fig. 7).[50] GQDs were formed by electrochemical oxidation of a graphene electrode in phosphate buffer solution. The oxygen containing groups on the surface of the GQDs provided aqueous solubility and facilitated further surface functionalization. Their topographic heights were between 1 and 2 nm, GQDs produced by electrochemical oxidation were made of 1–3 graphene layers, attributed to strong intergraphene attraction.[51]

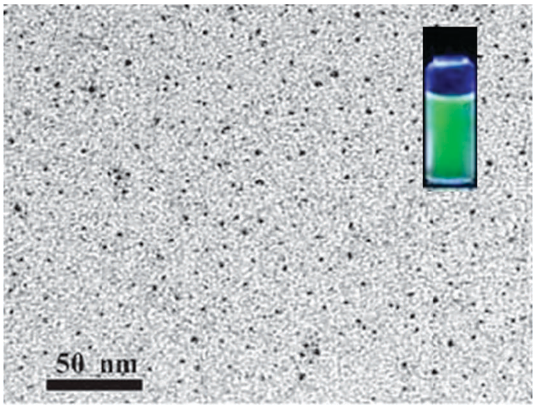

Fig. 7 TEM images of green-luminescent GQDs prepared by electrochemical oxidation of a graphene electrode in phosphate buffer solution, inset is a photo of a GQD aqueous solution under UV irradiation (365 nm). Reprinted with permission from ref. 50. Copyright 2011.

2.1.3. Oxygen plasma treatment. Another top-down method was discovered by Gokus *et al.*, who claimed that strong PL could be induced in single-layer graphene (SLG) using an oxygen plasma.[52] The PL was spatially uniform across the flakes and connected to elastic scattering spectra distinctly different from those of gapless pristine graphene. Oxygen plasma could be used to selectively convert the topmost layer when multilayer samples were treated. Briefly, graphene samples produced by microcleavage of graphite on a silicon substrate were exposed to oxygen : argon (1 : 2) RF plasma (0.04 mbar, 10 W) for increasing time (1–6 s). The structural and optical changes were monitored by Raman spectroscopy and elastic light scattering.[53,54] The PL decay dynamics was recorded by time-correlated single photon counting (TCSPC) upon pulsed excitation at 530 nm. The results showed that confocal PL maps revealed bright, pointlike PL features for short treatment times (1–3 s), whereas for slightly longer exposures (5–6 s) spatially uniform broadband visible PL was observed across SLG flakes (Fig. 8a and b). Moreover, another group discovered that the GO nanosheets possessed visible and near-infrared (vis-NIR) fluorescene.[55] Further, the fluorescence intensity was dependent on the ionic strength and pH (Fig. 8c and d). Extracellular pH evolution during the growth and metabolism of normal and cancer cells has been

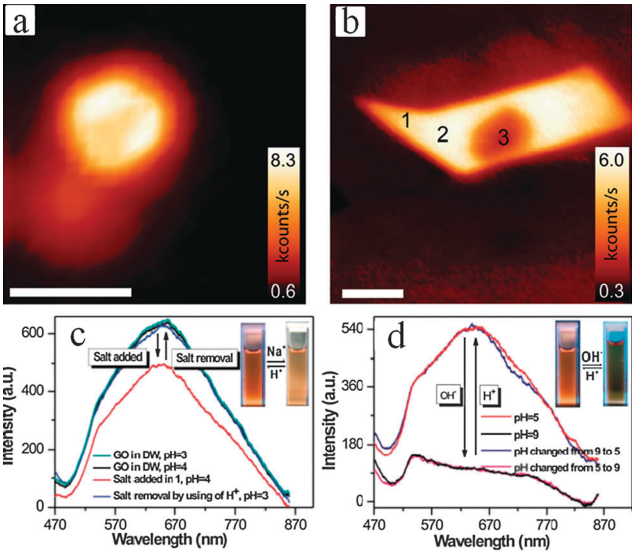

Fig. 8 (a) Confocal PL image excited at 473 nm (2.62 eV) for a graphene sample oxidized for 3 s. Scale bar = 5 μm. The bright PL spots are spatially localized. (b) Uniform emission after 5 s; scale bar = 10 μm. (c) Reversibility of the salt effect (inset: photograph of a reversible vis-NIR fluorescence change between acidic and salt conditions). (d) Reversibility of the pH effect (inset: photograph of a reversible vis-NIR fluorescence change between acidic and alkaline conditions). Reprinted with permission from refs. 52 and 55. Copyright 2009 and 2011.

monitored by GO nanosheets while vis-NIR fluorescence of GO has been further applied in bioimaging and optical chemo/biosensing.

2.2. Bottom-up approaches

2.2.1. Cage-opening of fullerene. At present, some groups have independently reported appealing methods for graphene nanoribbons production by the gradual unzipping of the carbon nanotubes.[56,57] Graphitic carbon layers can be derived from the surface-catalysed decomposition of fullerene adlayers on reactive transition metals. Loh *et al*. reported a mechanistic approach to the synthesis of a series of atomically defined GQDs by metal-catalysed cage-opening of C_{60} (Fig. 9).[58] The fragmentation of the embedded molecules at elevated temperatures produced carbon clusters that underwent diffusion and aggregation to form graphene quantum dots. The equilibrium shape of the graphene could be tailored by optimizing the annealing temperature and the density of the carbon clusters. Loh *et al*. tracked the evolution of a lone C_{60} molecule on Ru(0001). When the substrate covered with 0.03 ML C_{60} was gently heated to 450 K for 10 min, the C_{60} transformed into structures with threefold rotational symmetry. After flash annealing for 2 min at 725 K, numerous bright spots that were distinctly different from the starting C_{60} were found on the surface. The apparent height for these bright spots was 2.7 Å, representing a decrease of 60% from the initial height of 6.5 Å for C_{60} under a similar bias voltage. Annealing to 725 K produced flower-shaped dots with a threefold symmetry (0.7 nm), which constituted ∼23% of the decomposition products. Hexagonal mushroom-shaped dots with a lateral width of 0.9 nm were also observed with a 67% yield. After annealing at 825 K, the smaller flower-shaped dots appeared to have merged into larger ones (1.2 nm). The magnified view of a 1.2 nm dot showed that it originated from the combination of three flower-shaped dots, which were joined at a central protrusion spot.

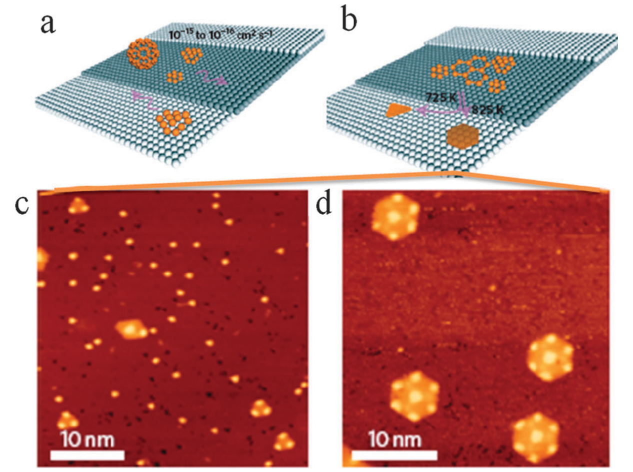

Fig. 9 Comparison of the growth mechanism of GQDs using C_{60}. (a) The majority of C_{60} molecules adsorb on the terraces and these decompose to produce carbon clusters with restricted mobility. (b) Temperature-dependent growth of GQDs with different equilibrium shapes from the aggregation of surface diffused carbon clusters. (c, d) Corresponding STM images for the well-dispersed triangular and hexagonal equilibrium shaped GQDs produced from C_{60}-derived carbon clusters. Tunnelling parameters (c, d): V = 0.5 V, I = 1 nA. Reprinted with permission from ref. 58. Copyright 2011.

2.2.2. Solution chemistry methods. For the bottom-up approach, solution-phase chemical methods by oxidative condensation of aryl groups have been successfully applied to produce GQDs.[51,59–65] Although it had been demonstrated that intramolecular oxidative cyclodehydrogenation was useful for the synthesis of large polycyclic aromatic hydrocarbons (PAHs) from dendritic arene precursors, the solubility of such GQDs was unfortunately low and they exhibited a tendency to aggregate due to strong intergraphene attraction.[66–68] Li *et al.* reported the synthesis of stabilized GQDs with uniform and tunable size by multiple 2′,4′,6′-trialkyl phenyl groups covalently attached to the edges of the graphene moieties.[59] Their as-prepared GQDs consist of graphene moieties containing 168, 132 or 170 conjugated carbon atoms, respectively (Fig. 10a). The formation of 3-D protection was attributed to the strong covalent binding and twisted phenyl groups due to crowdedness at the edge of the graphene moieties. They reported a stepwise solution chemistry route for the synthesis of these GQDs, which is illustrated in Fig. 10b.

Very recently, Liu *et al.* prepared multicolor GQDs with a uniform size of ∼60 nm diameter and 2–3 nm thickness by using unsubstituted hexa-*peri*-hexabenzocoronene (HBC) as the precursor (Fig. 11a and b).[65] The as-prepared GQDs with ordered morphology were obtained by pyrolysis and exfoliation of large PAHs, and the morphology of the GQDs were influenced by the pyrolysis temperature. Fig. 11c shows the scheme of the overall procedure for the preparation of GQDs. The as-made powder of HBC was first pyrolyzed at a high temperature. Then the artificial graphite was oxidized and exfoliated with a modified Hummers method.[69] Finally, aqueous solutions of the resultant GOs were heated to reflux for 48 h with oligomeric PEG_{1500N} and then reduced with hydrazine.

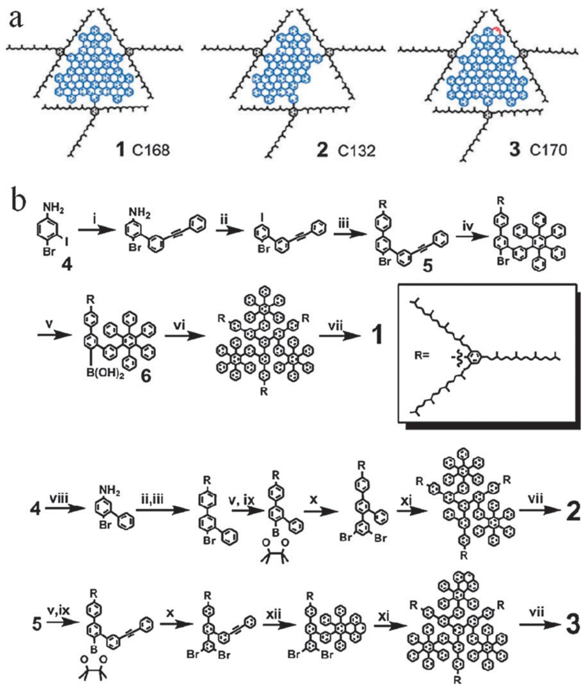

Fig. 10 (a) Schemes of colloidal GQDs with tunable size. (b) Synthesis of GQDs *via* a wet chemistry approach. Reprinted with permission from ref. 59. Copyright 2010.

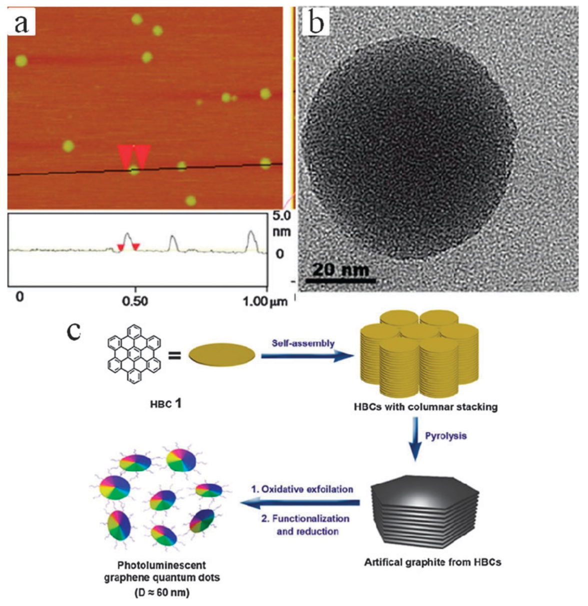

Fig. 11 (a) AFM topography images of GQD-1200 on mica substrates. (b) TEM images of GQD-1200. (c) Processing diagram for the preparation of photoluminescent GQDs using HBC as the carbon source. Reprinted with permission from ref. 65. Copyright 2011.

3. Physical and chemical properties

3.1. Optical properties

3.1.1. Photoluminescence. GQDs typically show strong optical absorption in the UV region, with a tail extending out into the visible range. The PL spectra are generally broad and dependent on excitation wavelength, the PL peaks shifted to longer wavelengths with a maximum intensity as the excitation wavelength was changed from 300 to 470 nm; the strongest peak was excited at 360 nm which emitted bright blue photoluminescence (Fig. 12a).[40,42,44,45] The PL spectrum can be considered as a transition from the lowest unoccupied molecular orbital (LUMO) to the highest occupied molecular orbital (HOMO). Fig. 12b shows the dependence of the HOMO–LUMO gap on the size of the graphene fragments.[45,70] Since the gap decreases gradually as the size of GQDs increases, sample mixtures of different particle size GQDs have different excitation and emission spectra, which is in agreement with previous reports. Some groups have prepared smaller GQDs (3–5 nm average diameter), which possess strong green fluorescence (Fig. 12c).[43,50]

In addition to the size of the graphene fragments, the pH of the GQDs solution will also influence the PL intensity. As Pan *et al.* reported,[42] under alkaline conditions, the GQDs emitted strong PL whereas, under acidic conditions, the PL was nearly completely quenched. If pH was switched repeatedly between 13 and 1, the PL intensity varies reversibly. However, this bahaviour may limit the applications of GQDs. Shen *et al.* presented GQDs surface passivated by PEG to solve this problem. They exhibited bright PL in a water solution of neutral pH[44] while the intensity of the PL peaks decreased by only about 25% under both acidic and alkaline conditions. They further found that as-prepared GQDs-PEG showed excellent luminescence properties, and the PL quantum yield with 360 nm emission was 28.0%, which was two times higher than for the pure GQDs. Due to the surface-passivation agent,

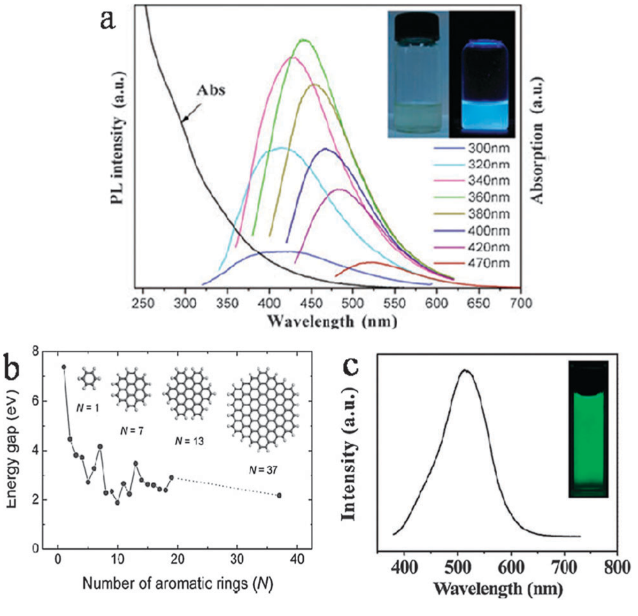

Fig. 12 (a) UV-vis absorption (Abs) and PL spectra of GQDs at different excitation wavelengths. Inset: photograph of a GQD aqueous solution taken under visible light and 365 nm UV light, from left to right, respectively. (b) Energy gap of π–π* transitions calculated based on DFT as a function of the number (*N*) of fused aromatic rings. The inset shows the structures of the graphene molecules used for calculation. (c) PL (at 375 nm excitation) spectra of a GQD aqueous solution (inset: photograph taken under UV light). Reprinted with permission from refs. 44, 45 and 43. Copyright 2010 and 2011.

there must be a higher quantum confinement of emissive energy trapped to the GQDs surface so that the GQDs with surface-passivation exhibit stronger PL.[71]

Besides the factors described above, there are other factors that can influence the PL performance. As Chhowalla reported the PL intensity was found to vary with reduction treatment by hydrazine vapor, which can be correlated to the evolution of very small sp^2 clusters.[45] Gokus *et al.* discovered the PL intensity and thickness of graphene were directly correlated, as seen in Fig. 13 for flakes of different thickness.[52] The single-layer graphene showed pronounced PL, but a different behavior was observed for multilayer graphene. Oxygen plasma etching proceeds layer-by-layer, and bi- and multilayer flakes remained nonluminescent, thus implying that emission from the topmost layer was quenched by subjacent untreated layers.

3.1.2. Upconversion luminescence. Upconversion fluorescence materials have attracted much recent attention for their many promising applications, especially in the growing field of biomedical imaging. However, the upconversion photoluminescence (UCPL) of GQDs were little researched until recently. In 2008, Sun and co-workers discovered the C-dots were found to be strongly emissive in the visible region with either argon-ion laser excitation (458 nm) or a femtosecond pulsed laser for two-photon excitation in the near-infrared (800 nm).[72] In addition, available results from exploratory experiments of luminescence imaging *in vitro* suggested that the C-dots were internalized into human breast cancer cells likely through endocytosis, demonstrating the potential of the C-dots in cell imaging with two-photon luminescence microscopy. After this, Lee *et al.* prepared C-dots by an alkali-assisted electrochemical method, which possessed size-dependent PL and excellent upconversion luminescence (UCPL) properties.[70] They also proposed that the UCPL property of C-dots should be attributed to the multiphoton active process similar to that reported above, and that combining C-dots with catalytic TiO_2 in a composite system for photocatalysis would realize the efficient usage of the full spectrum of sunlight. However, Shen *et al.* proposed that the multiphoton active process was not sufficient to explain their experimental phenomenon.[44] As shown in Fig. 14a, the PL spectrum of GQDs excited by a 980 nm laser showed upconverted green light emission. Upon changing the excitation wavelength from 600 to 800 nm, the upconverted emissions peak shifted from 390 to 468 nm, respectively (Fig. 14b). Remarkably, the shifting between the energy of upconverted emission light (E_m) and excitation light (E_x) was almost unchanged, about 1.1 eV. To further confirm and explain these experimental observations, an energy level structural model of the GQDs was proposed to investigate the UCPL properties. UCPL was speculated as due to anti-Stokes photoluminescence (ASPL), where ΔE between the π and σ orbitals was near 1.1 eV. The energy levels of π and σ orbitals were determined by the carbene ground-state multiplicity.[73–75] As shown in Fig. 14c, when a number of low-energy photons excite the electrons of the π orbital, the π electrons would undergo transition to a higher energy state such as the LUMO, and then the electrons would relax back to a lower energy state. Thus, an upconverted PL is emitted when the electrons return back to the σ orbital. Although the electrons of the σ orbital can also undergo transition they only can emit normal PL.

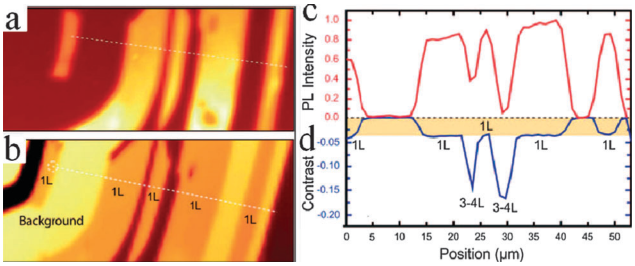

Fig. 13 Correlation between PL and layer thickness. (a) Confocal PL image; (b) elastic scattering image of the same sample area; (c, d) corresponding cross-sections taken along the dashed lines in (a, b). PL is only observed from treated SLG (marked 1 L here); 3–4 L denotes a multilayer. Reprinted with permission from ref. 52. Copyright 2009.

3.2. Cytotoxicity

As reported, C-dots have low toxicity[12,76,77] and the cytotoxicity of GQDs has been studied by various research groups. Dai and co-workers have also studied the cytotoxicity of nanographene oxide sheet-PEG composites by incubating Raji cells in various concentrations for 72 h, as shown in Fig. 15a.[41] They observed slight reductions of cell viability only for extremely high concentrations (>100 mg L^{-1}). Additionally, Yang and co-workers performed studies using MG-63 cells[43] and also found GQDs possessed low cytotoxicity. Adding up to 400 mg of GQDs to 150 mL of culture medium (104 cells) did not weaken the cell activity significantly, as shown by MTT assay (Fig. 15b). The result indicated the as-prepared GQDs could be used in bioimaging and other biomedical applications at high concentration.

All the evidence shows that GQDs have great potential for *in vitro* and *in vivo* imaging studies. Although further toxicity studies need to be carried out, such as LD50 (median lethal dose) measurements, some researchers predict that the biocompatibility

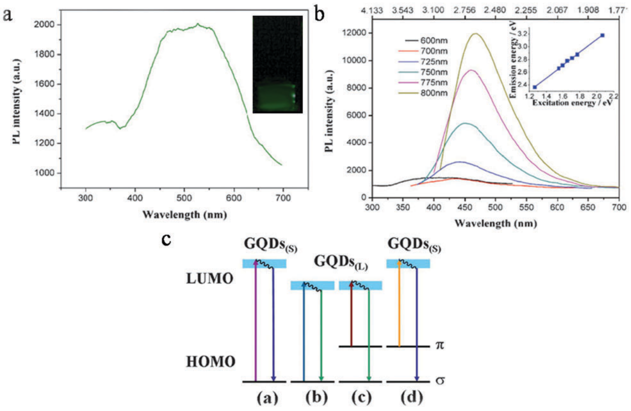

Fig. 14 (a) PL spectrum excited by 980 nm laser. Inset: Photograph of the GQD aqueous solution taken under 980 nm laser. (b) Upconverted PL properties of GQDs, inset is the energy of the excitation light as a function of the emission according to $E_m = 1.00E_x + \Delta E$ ($R^2 = 0.9983$) with $\Delta E = 1.1$ eV. (c) A schematic illustration of various typical electronic transition processes of GQDs. Reprinted with permission from ref. 44. Copyright 2011.

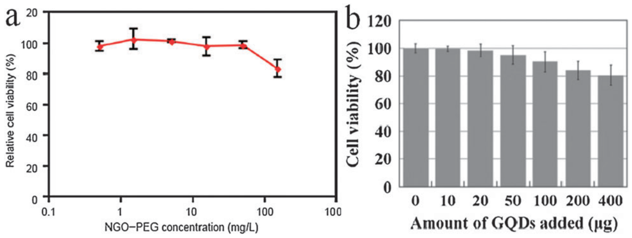

Fig. 15 (a) Dosage-dependent cellular toxicity of NGO PEG to Raji cells. Relative cell viabilities *vs.* untreated control were plotted against NGO PEG concentrations. No obvious toxicity was observed except a slight delay of cell growth at the highest NGO PEG concentration (150 mg L^{-1}). (b) Effect of GQDs on MG-63 cell viability. Reprinted with permission from refs. 41 and 43. Copyright 2008 and 2011.

of the carbon fluorescent materials will lead to replacement of current FDA-approved dyes used as optical imaging agents, such as indocyanine green (LD50 = 60 mg kg^{-1} body weight).[77]

3.3. Other physical properties

Besides the properties described above, there are other excellent properties of GQDs due to the physical structure of graphene.[78–80] GQDs were shown to be both excellent electron donors and acceptors.[40,81] Li *et al.* prepared GQDs with a uniform and tunable size by solution chemistry methods, and showed some special properties of GQDs and their optoelectronic applications such as in photodetectors and solar cells.[59–64] They synthesized disk-shaped nanostructures materials by assembly the colloidal GQDs on polar surfaces and the control of their orientations. They showed that the orientations of the GQDs could be determined, either in- or out-of-plane with the substrate, by chemical functionalization that introduces orientation-dependent interactions between the quantum dots and the surfaces.[60] The orientation control of the GQDs could have practical significance in determining their performance in devices. For example, for use as sensitizers in dye-sensitized solar cells, orientation control through chemical functionalization could also be applied to aligning graphene nanoribbons to take advantage of their outstanding charge transport properties for electro-optical applications. In addition, Li *et al.* first reported on the studies of electronic energy relaxation pathways in colloidal GQDs with uniform size.[62] They discovered that the photoexcited GQDs had a significant probability of relaxing into triplet states and emitted both phosphorescence and fluorescence at room temperature, with relative intensities depending on the excitation energy. Because of the long lifetime and reactivity of triplet electronic states, they predicted that their results could have significant implications for applications of graphenes. Then, they showed that carrier cooling in GQDs could be two orders of magnitude slower than in bulk materials, which could enable harvesting of hot charge carriers to improve the efficiency of solar energy conversion.[64] The slow hot-carrier relaxation in GQDs made it possible to reveal other normally slow relaxation pathways that were otherwise difficult to observe. Intersystem crossing is generally much slower than internal conversion since it involves a change in spin multiplicity. It could be enhanced in GQDs due to the reduced singlet–triplet splitting in such large conjugated systems.[62] The prolonged lifetimes of hot carriers would further make it likely to be competitive against internal conversion. More interestingly, the reduced hot-carrier cooling rates could increase the efficiency of processes such as hot electron extraction or multiexciton generation, to improve the efficiency of photovoltaic devices.[82,83]

Graphene is metallic, leading to the possibility of modes where the structural and electronic degrees of freedom are entangled[84] and is thus an excellent candidate material for the manipulation of spins.[85] Although the mechanisms responsible for spin diffusion are not yet fully understood, graphene spintronics has been studied by many research groups.[85,86] The presence of adatoms or corrugations is found to modify the spin–orbit coupling in GQDs.[87,88] It could also be altered into multilayered graphene.[89] Recent measurements consistent with the presence of local moments in graphene have been reported and magnetism in GQDs has been the subject of extensive studies in recent years.[90–93] For example, Viana-Gomes *et al.* has studied magnetism in GQDs of particular geometries with and without zigzag edges. Similarly to what had been proposed in the context of graphene nanoribbons, the magnetism displayed by these systems may be used in spin filters.[90] A large number of theoretical works suggested that the formation of local moments were at GQD edges and other defects. The interactions between these local moments could be modified by gate voltages, dopants and other sources of disorder, and strains. The expected distribution of local moments at GQDs and graphene ribbon edges are shown in Fig. 16.

4. Applications

4.1. Bioimaging

Traditional semiconductor quantum dots such as CdSe or CdS and their core–shell nanoparticles have been used in various *in vitro* or *in vivo* optical imaging experiments.[94,95] However, these QDs dots have prompted serious health and environmental concerns due to the heavy metal elements in them.[95] As a consequence of their tunable and strong PL properties, established low toxicity and eco-friendly nature, GQDs are an attractive alternative for bioimaging applications.

Zhu and co-workers reported the use of a coaxial electrospray method to the one-step fabrication of multifunctional core–shell structured capsules, which possessed magnetic targeting and fluorescence imaging functions.[96] The TiO_2 shell suppressed the initial burst release of paclitaxel while Fe_3O_4 and GQDs inside the oil core functioned successfully for magnetic targeting and fluorescence imaging, respectively.

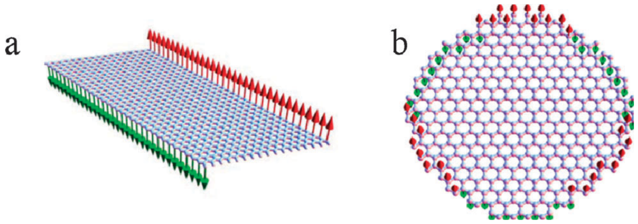

Fig. 16 (a) Sketch of the magnetization in a graphene ribbon with zigzag edges. (b) Magnetization near the edges of a graphene quantum dot. Reprinted with permission from ref. 84. Copyright 2011.

Furthermore, paclitaxel in capsules was trigger released by ultrasound stimulation, and the release profile could be controlled by the length of the repeatable ultrasound time. In order to achieve the integration of targeted, therapy and imaging, the capsules were designed in a multifunctional core–shell structure as shown in Fig. 17.

Dai and co-workers also reported the first study on nanographene oxide sheet cellular imaging and drug delivery capabilities.[41] The nanographene oxide sheets were found to be PL in the visible and infrared regions. They demonstrated intrinsic PL could be used for live cell imaging in the near-infrared (NIR) with little background. They also found that simple physisorption *via* π-stacking could be used for loading doxorubicin, a widely used cancer drug onto nanographene oxide sheets functionalized with antibodies for selective killing of cancer cells *in vitro*. As shown in Fig. 18a, Dai and co-workers covalently conjugated a B-cell specific antibody Rituxan (anti-CD20) to nanographene oxide PEG in order to selectively recognize and bind to B-cell lymphoma cells. B- and T-cells were incubated in solutions of nanographene oxide–PEG Rituxan conjugates at 4 °C to allow the conjugates to interact with the cell surface but block internalization *via* endocytosis.[97] The cells were imaged by detecting NIR PL in the range 1100–2200 nm using a InGaAs detector under 658 nm laser excitation (laser spot size ~1 μm, Fig. 18b and c). This confirmed selective nanographene oxide-PEG-Ab binding to B- over T-cells (Fig. 18d). Owing to its small size, intrinsic optical properties, large specific surface area, low cost, and useful non-covalent interactions with aromatic drug molecules, nanographene oxide is a promising new material for biological and medical applications.

Zhu *et al.* also used GQDs for conventional bioimaging by incubating a 10^4 cells/150 μL solution of MG-63 (human osteosarcoma) cells with suspensions (2.5 mg mL^{-1}) of GQDs from a stock solution with Dulbecco's phosphate buffer saline (DPBS).[43] MG-63 cells were cultured in Dulbecco's modified Eagle's medium supplemented with 10% fetal bovine serum and 1% penicillin/streptomycin (DMEM). The GQDs were produced by a one-step solvothermal method with PL quantum yield as high as 11.4%. Then, after sonication for 10 min to ensure complete dispersion, an aliquot (typically 0.01 mL) of the suspension was added to the well of a chamber slide containing the cells cultured for 24 h. The chamber slide was then incubated at 37 °C in a CO_2 incubator for 12 h for GQDs uptake (only 10 μg of GQDs to 150 μL of culture medium (10^4 cells) was added). Prior to fixation of the cells on the slide for inspection with a confocal fluorescence microscope, the excess GQDs were removed by washing three times with warm DPBS. GQDs uptake and bioimaging experiments were performed by the confocal fluorescence microscope as shown in Fig. 19. Observation of the bright green area inside the cells indicated translocation of GQDs through the cell's membrane (405 nm excitation). The excitation-dependent PL behavior of the GQDs gave rise to impressive visible results. When the excitation light was changed to 488 nm a green–yellow color was observed (Fig. 19c).

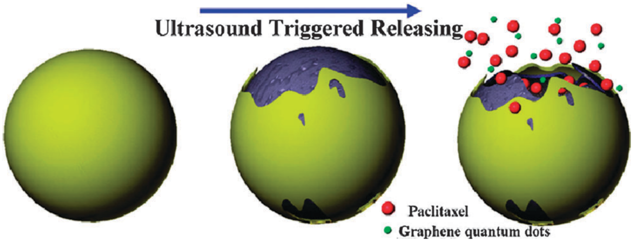

Fig. 17 Schematic illustration for procedures of shell cracking leading to drug release from capsules with increasing ultrasound time. Reprinted with permission from ref. 96. Copyright 2011.

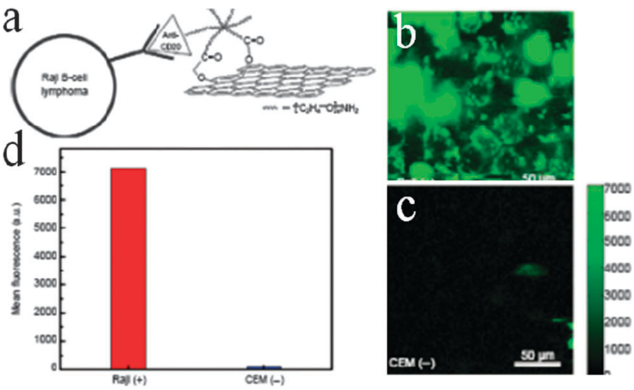

Fig. 18 Nanographene for targeted NIR imaging of live cells. (a) A schematic drawing illustrating the selective binding and cellular imaging of NGO PEG conjugated with anti-CD20 antibody, Rituxan. (b) NIR fluorescence image of CD20 positive Raji B-cells treated with the nanographene oxide PEG–Rituxan conjugate. The scale bar shows the intensity of total NIR emission (in the range 1100–2200 nm). Images are false-colored green. (c) NIR fluorescence image of CD20 negative CEM T-Cells treated with nanographene oxide PEG-Rituxan conjugate. (d) Mean NIR fluorescence intensities in the image area for the both the positive (Raji) and negative (CEM) cells treated by nanographene oxide PEG Rituxan conjugate. Reprinted with permission from ref. 41. Copyright 2008.

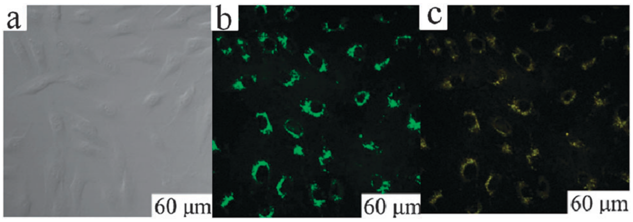

Fig. 19 Cellular imaging of GQDs; (a–c) are washed cells imaged under bright field, 405 and 488 nm excitations, respectively. Reprinted with permission from ref. 43. Copyright 2011.

As shown in previous publications, cellular toxicity data showed high biocompatibility and low toxicity of GQDs. However, further experiments should be provided for *in vitro* and *in vivo* applications, and for actual applications in the human body.

4.2. Electrochemical biosensors

Due to the excellent conductivity of GQDs, Li *et al.* had designed a simple but smart platform to fabricate electrochemical biosensors by using GQD-modified electrodes coupled with specific sequence ssDNA molecules as probes.[98] The probe ssDNA inhibited electron transfer between electrochemically active species $[Fe(CN)_6]^{3-/4-}$ and the electrode after the probe molecules were strongly bound to the surface of the modified electrode *via* their interaction with GQDs. However, when the target molecules such as target ssDNA or target protein were also present in the test solution, the probe ssDNA bound with the target instead of GQDs if the sequence of the probe ssDNA was designed as complementary to the target DNA or as the aptamer of the target protein. The obtained peak currents of $[Fe(CN)_6]^{3-/4-}$ increased with the target molecules, thus various electrochemical biosensors can be readily developed with this proposed platform. The fabricated electrochemical biosensors may also have high sensitivity and selectivity, which may have potential applications in the future.

4.3. Catalyst for the oxygen reduction reaction

Very recently, Qu *et al.* prepared nitrogen-doped GQDs (*N*-GQDs) with oxygen-rich functional groups by an electrochemical method using tetrabutylammonium perchlorate (TBAP) in acetontrile as electrolyte to introduce N atoms into the resultant GQDs *in situ*.[99] The doping of GQDs with heteroatoms provides an attractive means of effectively tuning their intrinsic properties and exploiting new phenomena for advanced device applications. Qu *et al.* reported that their as-prepared N-GQDs showed luminescent and electrocatalytically active properties. Unlike their N-free counterparts, the produced N-GQDs with a N/C atomic ratio of *ca.* 4.3% emitted blue luminescence and possessed an electrocatalytic activity comparable to that of a commercially available Pt/C catalyst for the oxygen reduction reaction (ORR) in alkaline medium (Fig. 20). In addition to their use as metal-free ORR catalysts in fuel cells, the linear-sweep voltammetry (LSV) curves of the ORR for NGQD/graphene in an O_2-saturated 0.1 M KOH solution were measured by a rotating disk electrode (RDE). The measured current density showed the typical increase with increasing rotation rate due to the enhanced diffusion of electrolytes.[100,101] Apart from the use of N-GQDs as a metal-free catalyst for ORR, their unique luminescence properties indicate their potential for use in bioimaging and light-emitting diodes, among many other potential applications.

4.4. Organic photovoltaic devices

Owing to their attractive optoelectronic properties and solution processibility, colloidal GQDs show promise of applications in low cost, upconversion PL and high performance photovoltaic devices (*e.g.*, organic/inorganic hybrid solar cells, GQD-sensitized solar cells and organic light emitting diodes).

Li *et al.* applied colloidal GQDs with green luminescence as electron-acceptor materials in conjugated polymer, poly(3-hexylthiophene) (P3HT)-based thin film solar cells.[50] Although without device optimization in this primary study, a power conversion efficiency of 1.28% was achieved. As shown in Fig. 21a, polymer photovoltaic cells with the structure of ITO|PEDOT:PSS|P3HT:GQDs|Al were fabricated (ITO, PEDOT, PSS and P3HT correspond to indium tin oxide, poly(3,4-ethylenedioxythiophene), poly(styrenesulfonate) and poly(3-hexylthiophene), respectively). The GQDs (10 wt%) provided an effective interface for charge separation and a pathway for electron transport, and the energy level diagram for the GQD-based photovoltaic cells is shown in Fig. 21b.

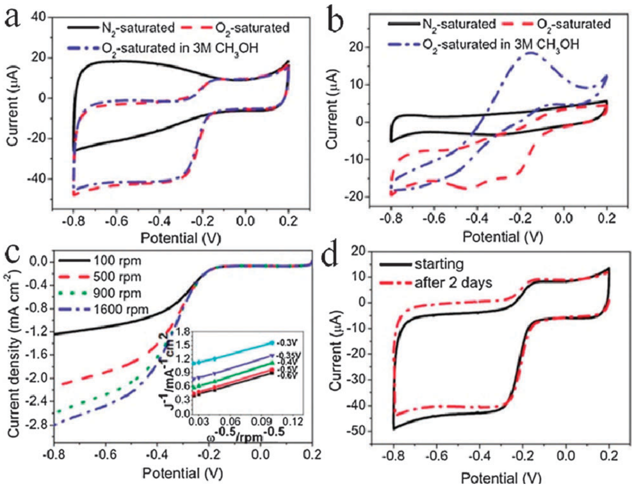

Fig. 20 (a, b) CVs of (a) N-GQD/graphene and (b) commercial Pt/C on a GC electrode in N_2-saturated 0.1 M KOH, O_2-saturated 0.1 M KOH, and O_2-saturated 3 M MeOH solutions. (c) Rotating-disk electrode (RDE) curves for N-GQD/graphene in O_2-saturated 0.1 M KOH with different speeds. The inset shows Koutecky–Levich plots derived from the RDE measurements. (d) Electrochemical stability of N-GQD/graphene as determined by continuous cyclic voltammetry in O_2-saturated 0.1 M KOH. Reprinted with permission from ref. 99. Copyright 2011.

Fig. 21c compares the current density–voltage (*J*–*V*) characteristics of a typical undoped P3HT device with those of one blended with GQDs before and after annealing in the dark and under illumination.

Yan *et al.* also reported that GQDs have high optical absorptivity and nearly optimized absorption in the visible and near-IR region.[63] Moreover, the calculated energy level in GQDs suggested the possibility of electron injection from GQDs to the large bandgap of TiO_2 upon photoexcitation and regeneration of GQDs by accepting an electron from I^-. GQDs thus provide unique opportunities for the development of inexpensive, high efficiency GQD-sensitized solar cells by substituting GQDs for metal-organic dyes as photosensitizers. Remarkably, since GQDs also were shown to possess UCPL properties, they would find significant applications in photoelectrochemical cells, especially for use in near-infrared light absorption. Zhu *et al.* studied the photon-to-electron conversion capability of GQDs.[40] The photocurrents generated by GQDs-PEG and GQDs on ITO electrodes were measured by a three-electrode system. As demonstrated in Fig. 22, the GQDs-PEG photoelectrode generated photocurrent with both 365 nm UV light and 808 nm NIR laser, while the pure GQD photoelectrode showed less than half of the photocurrent of the GQDs-PEG. It is speculated that GQDs can be a new solar cell dopant material and the light of the photon-to-electron conversion may be extended from the ultraviolet to the near infrared.

Gupta *et al.* demonstrated that GQDs blended with regioregular P3HT or poly(2-methoxy-5-(2-ethylhexyloxy)-1,4-phenylenevinylene) (MEH-PPV) polymer results in a significant improvement in the efficiency of solar cells or organic light emitting diode (OLED) characteristics as compared to graphene nanosheets (GS) blended conjugated polymers.[81] The GQDs were

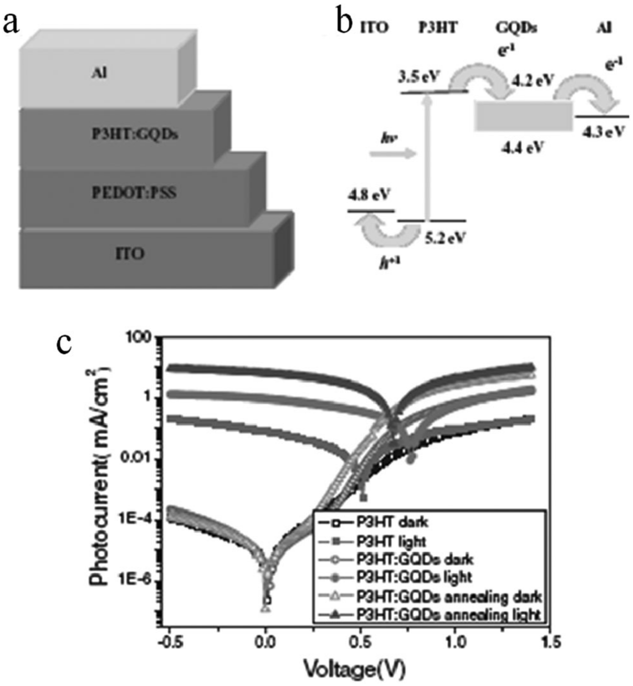

Fig. 21 Schematic (a) and energy band (b) diagrams of the ITO|PEDOT:PSS|P3HT:GQDs|Al device. (c) *J*–*V* characteristic curves for the ITO|PEDOT:PSS|P3HT|Al, ITO|PEDOT:PSS|P3HT:GQDs|Al and ITO|PEDOT:PSS|P3HT:GQDs|Al devices after annealing at 140 °C for 10 min (single log scale). Reprinted with permission from ref. 50. Copyright 2011.

synthesized from graphene nanosheets by the hydrothermal approach, which were functionalized with aniline (ANI) or methylene blue (MB) (ANI-GQDs and MB-GQDs). *J*–*V* curves of the ANI-GQD and ANI-GS (optimized) photovoltaic devices are plotted in Fig. 23a and corresponding band diagrams are given in the inset. A maximum η of 1.14, V_{oc} of 0.61 V, J_{sc} of 3.51 mA cm^{-2} and FF of 0.53 were obtained for 1 wt% ANI-GQD in P3HT. As shown in the inset, the LUMO and HOMO of GQDs were −3.55 and −5.38 eV, respectively, as determined by cyclic voltammetry. The position of the LUMO of GQDs in between that of P3HT1 and Al suggested their suitability for solar cell applications. Fig. 23b shows the *J*–*V* curves of the different OLEDs and the corresponding band diagrams are given in the inset. The turn-on voltage for the pure MEHPPV sample was about 6 V and was decreased to 4 V for MEHPPV|MB-GQDs (1 wt%). MEHPPV|MB-GQDs (1 wt%) exhibited strong yellow emission as compared to the bright orange emission of MEHPPV. The MB-GQDs dispersed in the MEHPPV provided more electrical transport paths, which results in an enhancement of charge injection and hence caused increase in the carrier density, thus requiring lower turn-on voltage and much higher efficiency.

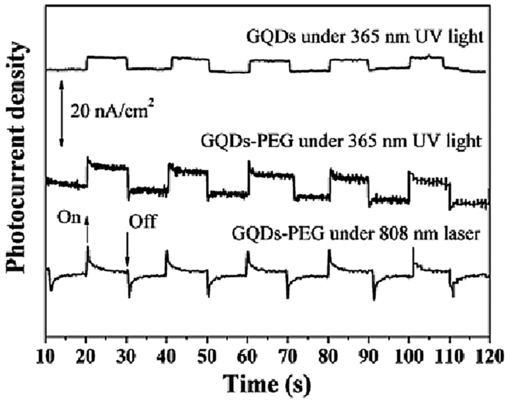

Fig. 22 Photocurrent response of GQDs-PEG and GQDs photoelectrodes under 365 nm UV light or 808 nm NIR laser. Reprinted with permission from ref. 40. Copyright 2011.

5. Outlook

Although much research for GQDs has been done the detailed mechanism and chemical species responsible for PL in GQDs derivatives still further understanding. Throughout these studies, some interesting questions arise such as the factors affecting the energy band of GQDs, whether significant inhomogeneity of the oxidation profile exists within the GO plane, and whether energy relaxation and spectral diffusion in GO-type materials are altered by aggregation and interlayer coupling. GQDs have received much attention as they may gradually replace traditional quantum semiconductors applied in bioimaging, disease detection, drug delivery and photovoltaic devices, due to their superiority in terms of chemical inertness, biocompatibility and low toxicity. However, GQDs also have some disadvantages,

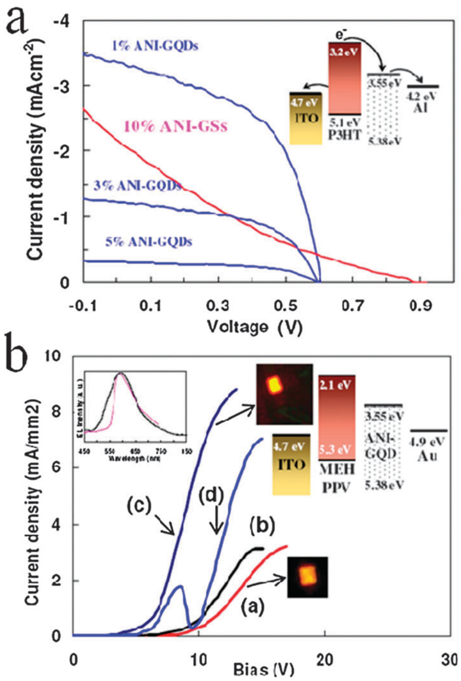

Fig. 23 (a) *J*–*V* characteristics of photovoltaic devices based on ANI-GQD with different GQD content and ANI-GS (under optimized condition) annealed at 160 °C for 10 min, in AM 1.5 G 100 mW illumination. (b) Measured current density of MEHPPV with MB-GQD: a: 0%, b: 0.5%, c: 1% and d: 3% as a function of the applied voltage (V). The inset plots the electroluminescence spectrum of MEHPPV (red) and MEHPPV|MB-GQD (1%) (black). The inset also shows the band diagram of MEHPPV|MB-GQD and the recorded brightness of MEHPPV LED and MEHPPV|MB-GQD(1%) LED. Reprinted with permission from ref. 81. Copyright 2011.

such as generally presenting a blue luminescence which was not conducive to biological imaging, and other luminescence including UCPL which is relatively weaker. In addition, solar cells with GQDs usually have relatively lower efficiency ($<2\%$). However the initial work on GQDs for solar cells or bioimaging are very promising. As discussed below, future research efforts towards better controlled synthesis, surface functionalization, metal enhanced fluorescence and new quantum dot materials are expected to result in even higher performance.

5.1. New methods for the synthesis of GQDs

Synthesis of high quality GQDs with well controlled size, shape and surface functionalization needs to be further explored. GQDs prepared by the top-down approaches are usually difficult to control in terms of size and shape. Therefore, we speculate the bottom-up methods will become the dominant development direction for the synthesis of GQDs. The concepts of confined reaction and nanoreactors, which has been used to prepare nanoparticles, may well be a useful area for research.

5.2. Surface engineering on GQDs

In contrast, the surface engineering of GQDs has been studied relatively less. The surface modification on GQDs has a great influence on their performance. Zhou *et al.* have introduced different shaped GQDs functioning as conjugated bridges in the donor–bridge–acceptor (NH_2-GQD-NO_2) systems.[102] They found that the shape effect and singlet diradical or multiradical character of GQDs had a key role in enlarging β_0. They speculated that their work may provide a theoretical guide to design smaller and higher-performance nanophotonic devices in the future. In addition, in GQD-sensitized solar cells, the poor affinity between GQDs and the semiconductor surface is responsible for the quite low photocurrent; surface engineering of GQDs will be a good method to improve the performance of solar cells.

5.3. Metal enhanced fluorescence

GQDs have found application in many fields but are restricted by low quantum yields. The use of metal-enhanced fluorescence may well overcome some problems. Metal nanoparticles have attracted particular interest because of their fascinating electronic and optical properties. It has also been found that metal nanoparticles can affect fluorescence quenching or enhancement, which depends on the distance between the nanoparticles and fluorophore; small distances results in quenching while separation by certain larger distances causes enhancement.[103,104] Yang *et al.* have developed mesoporous nanocarriers consisting of a silver core, a silica spacer with controlled thickness and a fluorophore-loaded mesoporous silica shell for metal-enhanced fluorescence (MEF) and Förster resonance energy transfer (FRET) effects.[105] We can design structures where GQDs are located on metal@silica composite nanoparticles and the fluorescence of GQDs absorbed or emitted match the metal localized surface plasmon resonance (LSPR) absorption band, and an increase in thickness of the spacer layer (shell thickness) will enable a continuous transition from fluorescence quenching to fluorescence enhancement.

5.4. Newer quantum dot materials

In addition to C-dots and GQDs, many newer quantum dots have been discovered and researched recently, such as *h*-BN nanosheets or BCNO nanoparticles,[106] nanodiamonds,[107] fluorescent silicon quantum dots (SiQDs)[108–110] and so on. He *et al.* presented a microwave-assisted method for one-pot synthesis of water-dispersible SiQDs using silicon nanowires and glutaric acid as precursors.[110] Their prepared SiQDs, which feature excellent aqueous dispersibility, robust photo- and pH-stability, strong fluorescence (about 15%), and favorable sizes (about 4 nm), were readily and rapidly prepared in short reaction times. We speculate that the new quantum dot materials may provide biological probes for long-term and real-time immunofluorescent cellular imaging, which can overcome the disadvantages of GQDs.

Acknowledgements

We thank the National Natural Science Foundation of China (20925621, 20976054, and 21176083), the Special Projects for Nanotechnology of Shanghai (11nm0500800) the Fundamental Research Funds for the Central Universities, and the Program for Changjiang Scholars and Innovative Research Team in University (IRT0825), and the Shanghai Leading Academic Discipline Project (project number: B502) for financial support.

References

1 Y. Wang and L. Chen, *Nanomed.: Nanotechnol., Biol. Med.*, 2011, **7**, 385–402.
2 A. P. Alivisatos, *Science*, 1996, **271**, 933–937.
3 A. Priyam, D. E. Blumling and K. L. Knappenberger, *Langmuir*, 2010, **26**, 10636–10644.
4 F. Guo, Y. Zhu, X. Yang and C. Li, *Mater. Chem. Phys.*, 2007, **105**, 315–319.
5 P. Wang, Y. Zhu, X. Yang, C. Li and H. L. Du, *Acta Mater.*, 2008, **56**, 1144–1150.
6 Y. Li, Y. Zhu, X. Yang and C. Li, *Cryst. Growth Des.*, 2008, **8**, 4494–4498.
7 X. G. Peng, M. C. Schlamp, A. V. Kadavanich and A. P. Alivisatos, *J. Am. Chem. Soc.*, 1997, **119**, 7019–7029.
8 Y. W. Cao and U. Banin, *J. Am. Chem. Soc.*, 2000, **122**, 9692–9702.
9 B. A. Korgel and H. G. Monbouquette, *Langmuir*, 2000, **16**, 3588–3594.
10 A. L. Rogach, M. T. Harrison, S. V. Kershaw, A. Kornowski, M. G. Burt, A. Eychmuller and H. Weller, *Phys. Status Solidi B*, 2001, **224**, 153–158.
11 R. E. Bailey and S. Nie, *J. Am. Chem. Soc.*, 2003, **125**, 7100–7106.
12 S. T. Yang, L. Cao, P. G. Luo, F. S. Lu, X. Wang, H. F. Wang, M. J. Meziani, Y. F. Liu, G. Qi and Y. P. Sun, *J. Am. Chem. Soc.*, 2009, **131**, 11308–11309.
13 S. N. Baker and G. A. Baker, *Angew. Chem., Int. Ed.*, 2010, **49**, 6726–6744.
14 S. L. Hu, K. Y. Niu, J. Sun, J. Yang, N. Q. Zhao and X. W. Du, *J. Mater. Chem.*, 2009, **19**, 484–488.
15 Y. P. Sun, X. Wang, F. S. Lu, L. Cao, M. J. Meziani, P. J. G. Luo, L. R. Gu and L. M. Veca, *J. Phys. Chem. C*, 2008, **112**, 18295–18298.
16 J. G. Zhou, C. Booker, R. Y. Li, X. T. Zhou, T. K. Sham, X. L. Sun and Z. F. Ding, *J. Am. Chem. Soc.*, 2007, **129**, 744–745.
17 R. L. Liu, D. Q. Wu, S. H. Liu, K. Koynov, W. Knoll and Q. Li, *Angew. Chem., Int. Ed.*, 2009, **48**, 4598–4601.
18 J. G. Zhou, C. Booker, R. Y. Li, X. L. Sun, T. K. Sham and Z. F. Ding, *Chem. Phys. Lett.*, 2010, **493**, 296–298.
19 D. Y. Pan, J. C. Zhang, Z. Li, C. Wu, X. M. Yan and M. H. Wu, *Chem. Commun.*, 2010, **46**, 3681–3683.

20 A. B. Bourlinos, A. Stassinopoulos, D. Anglos, R. Zboril, V. Georgakilas and E. P. Giannelis, *Chem. Mater.*, 2008, **20**, 4539–4541.
21 H. P. Liu, T. Ye and C. Mao, *Angew. Chem., Int. Ed.*, 2007, **46**, 6473–6475.
22 L. Tian, D. Ghosh, W. Chen, S. Pradhan, X. J. Chang and S. W. Chen, *Chem. Mater.*, 2009, **21**, 2803–2809.
23 S. J. Yu, M. W. Kang, H. C. Chang, K. M. Chen and Y. C. Yu, *J. Am. Chem. Soc.*, 2005, **127**, 17604–17605.
24 H. Zhu, X. L. Wang, Y. L. Li, Z. J. Wang, F. Wang and X. R. Yang, *Chem. Commun.*, 2009, 5118–5120.
25 M. Bottini, C. Balasubramanian, M. I. Dawson, A. Bergamaschi, S. Bellucci and T. Mustelin, *J. Phys. Chem. B*, 2006, **110**, 831–836.
26 X. Wang, L. Cao, F. S. Lu, M. J. Meziani, H. Li, G. Qi, B. Zhou, B. A. Harruff, F. Kermarrec and Y. P. Sun, *Chem. Commun.*, 2009, 3774–3776.
27 L. Tian, Y. Song, X. J. Chang and S. W. Chen, *Scr. Mater.*, 2010, **62**, 883–886.
28 J. Zong, Y. H. Zhu, X. L. Yang, J. H. Shen and C. Z. Li, *Chem. Commun.*, 2011, **47**, 764–766.
29 K. Zhou, Y. Zhu, X. Yang and C. Li, *New J. Chem.*, 2010, **34**, 2950–2955.
30 K. Zhou, Y. Zhu, X. Yang and C. Li, *Electroanalysis*, 2011, **23**, 862–869.
31 J. Shen, Y. Zhu, K. Zhou, X. Yang and C. Li, *J. Mater. Chem.*, 2012, **22**, 545–550.
32 K. Zhou, Y. Zhu, X. Yang, J. Luo, C. Li and S. Luan, *Electrochim. Acta*, 2010, **55**, 3055–3060.
33 K. Zhou, Y. Zhu, X. Yang, X. Jiang and C. Li, *New J. Chem.*, 2011, **35**, 353–359.
34 K. Zhou, Y. Zhu, X. Yang and C. Li, *Electroanalysis*, 2010, **22**, 259–264.
35 A. K. Geim, *Science*, 2009, **324**, 1530–1534.
36 S. Stankovich, D. A. Dikin, G. H. B. Dommett, K. M. Kohlhaas, E. J. Zimney, E. A. Stach, R. D. Piner, S. B. T. Nguyen and R. S. Ruoff, *Nature*, 2006, **442**, 282–286.
37 X. J. Xie, H. Bai, G. Q. Shi and L. T. Qu, *J. Mater. Chem.*, 2011, **21**, 2057–2059.
38 K. Nakada, M. Fujita, G. Dresselhaus and M. S. Dresselhaus, *Phys. Rev. B: Condens. Matter*, 1996, **54**, 17954–17961.
39 Y. W. Son, M. L. Cohen and S. G. Louie, *Phys. Rev. Lett.*, 2006, **97**, 216803–216806.
40 J. Shen, Y. Zhu, X. Yang, J. Zong, J. Zhang and C. Li, *New J. Chem.*, 2012, **36**, 97–101.
41 X. Sun, Z. Liu, K. Welsher, J. T. Robinson, A. Goodwin, S. Zaric and H. Dai, *Nano Res.*, 2008, **1**, 203–212.
42 D. Pan, J. Zhang, Z. Li and M. Wu, *Adv. Mater.*, 2010, **22**, 734–738.
43 S. Zhu, J. Zhang, C. Qiao, S. Tang, Y. Li, W. Yuan, B. Li, L. Tian, F. Liu, R. Hu, H. Gao, H. Wei, H. Zhang, H. Sun and B. Yang, *Chem. Commun.*, 2011, **47**, 6858–6860.
44 J. Shen, Y. Zhu, C. Chen, X. Yang and C. Li, *Chem. Commun.*, 2011, **47**, 2580–2582.
45 G. Eda, Y.-Y. Lin, C. Mattevi, H. Yamaguchi, H.-A. Chen, I.-S. Chen, C.-W. Chen and M. Chhowalla, *Adv. Mater.*, 2010, **22**, 505–509.
46 J. Robertson and E. P. O'Reilly, *Phys. Rev. B*, 1987, **35**, 2946–2957.
47 Q. L. Zhao, Z. L. Zhang, B. H. Huang, J. Peng, M. Zhang and D. W. Pang, *Chem. Commun.*, 2008, 5116–5118.
48 L. Zheng, Y. Chi, Y. Dong, J. Lin and B. Wang, *J. Am. Chem. Soc.*, 2009, **131**, 4564–4565.
49 J. Lu, J. X. Yang, J. Z. Wang, A. Lim, S. Wang and K. P. Loh, *ACS Nano*, 2009, **3**, 2367–2375.
50 Y. Li, Y. Hu, Y. Zhao, G. Shi, L. Deng, Y. Hou and L. Qu, *Adv. Mater.*, 2011, **23**, 776–780.
51 J. Wang, X. Xin and Z. Lin, *Nanoscale*, 2011, **3**, 3040–3048.
52 T. Gokus, R. R. Nalr, A. Bonettl, M. Bohmler, A. Lombardo, K. S. Novoselov, A. K. Gelm, A. C. Ferrarl and A. Hartschuh, *ACS Nano*, 2009, **3**, 3963–3968.
53 C. Casiraghi, A. Hartschuh, E. Lidorikis, H. Qian, H. Harutyunyan, T. Gokus, K. S. Novoselov and A. C. Ferrari, *Nano Lett.*, 2007, **7**, 2711–2717.
54 A. C. Ferrari, J. C. Meyer, V. Scardaci, C. Casiraghi, F. Mauri, S. Piscanec, S. Piscanec, D. Jiang, K. S. Novoselov, S. Roth and A. K. Geim, *Phys. Rev. Lett.*, 2006, **97**, 187401–187404.
55 J.-L. Chen and X.-P. Yan, *Chem. Commun.*, 2011, **47**, 3135–3137.
56 D. V. Kosynkin, A. L. Higginbotham, A. Sinitskii, J. R. Lomeda, A. Dimiev, B. K. Price and J. M. Tour, *Nature*, 2009, **458**, 872–876.
57 L. Jiao, L. Zhang, X. Wang, G. Diankov and H. Dai, *Nature*, 2009, **458**, 877–880.
58 J. Lu, P. S. E. Yeo, C. K. Gan, P. Wu and K. P. Loh, *Nat. Nanotechnol.*, 2011, **6**, 247–252.
59 X. Yan, X. Cui and L.-S. Li, *J. Am. Chem. Soc.*, 2010, **132**, 5944–5945.
60 I. P. Hamilton, B. Li, X. Yan and L.-S. Li, *Nano Lett.*, 2011, **11**, 1524–1529.
61 L.-S. Li and X. Yan, *J. Phys. Chem. Lett.*, 2010, **1**, 2572–2576.
62 M. L. Mueller, X. Yan, J. A. McGuire and L.-S. Li, *Nano Lett.*, 2010, **10**, 2679–2682.
63 X. Yan, X. Cui, B. S. Li and L.-S. Li, *Nano Lett.*, 2010, **10**, 1869–1873.
64 M. L. Mueller, X. Yan, B. Dragnea and L.-S. Li, *Nano Lett.*, 2011, **11**, 56–60.
65 R. Liu, D. Wu, X. Feng and K. Mullen, *J. Am. Chem. Soc.*, 2011, **133**, 15221–15223.
66 C. D. Simpson, J. D. Brand, A. J. Berresheim, L. Przybilla, H. J. Rader and K. Mullen, *Chem.–Eur. J.*, 2002, **8**, 1424–1429.
67 J. Wu, W. Pisula and K. Mullen, *Chem. Rev.*, 2007, **107**, 718–747.
68 J. Wu, Z. Tomovic, V. Enkelmann and K. Mullen, *J. Org. Chem.*, 2004, **69**, 5179–5186.
69 W. S. Hummers and R. E. Offeman, *J. Am. Chem. Soc.*, 1958, **80**, 1339–1339.
70 H. T. Li, X. D. He, Z. H. Kang, H. Huang, Y. Liu, J. L. Liu, S. Y. Lian, C. H. A. Tsang, X. B. Yang and S. T. Lee, *Angew. Chem., Int. Ed.*, 2010, **49**, 4430–4434.
71 Y. P. Sun, B. Zhou, Y. Lin, W. Wang, K. A. S. Fernando, P. Pathak, M. J. Meziani, B. A. Harruff, X. Wang, H. F. Wang, P. J. G. Luo, H. Yang, M. E. Kose, B. Chen, L. M. Veca and S. Y. Xie, *J. Am. Chem. Soc.*, 2006, **128**, 7756–7757.
72 L. Cao, X. Wang, M. J. Meziani, F. Lu, H. Wang, P. G. Luo, Y. Lin, B. A. Harruff, L. M. Veca, D. Murray, S.-Y. Xie and Y.-P. Sun, *J. Am. Chem. Soc.*, 2007, **129**, 11318–11319.
73 L. R. Radovic and B. Bockrath, *J. Am. Chem. Soc.*, 2005, **127**, 5917–5927.
74 A. Mehta, E. J. Nelson, S. M. Webb and J. K. Holt, *Adv. Mater.*, 2009, **21**, 102–106.
75 A. M. Trozzolo and W. A. Gibbons, *J. Am. Chem. Soc.*, 1967, **89**, 239–243.
76 S. C. Ray, A. Saha, N. R. Jana and R. Sarkar, *J. Phys. Chem. C*, 2009, **113**, 18546–18551.
77 S.-T. Yang, X. Wang, H. Wang, F. Lu, P. G. Luo, L. Cao, M. J. Meziani, J.-H. Liu, Y. Liu, M. Chen, Y. Huang and Y.-P. Sun, *J. Phys. Chem. C*, 2009, **113**, 18110–18114.
78 S. Guo and S. Dong, *Chem. Soc. Rev.*, 2011, **40**, 2644–2672.
79 L. J. Cote, J. Kim, V. C. Tung, J. Luo, F. Kim and J. Huang, *Pure Appl. Chem.*, 2011, **83**, 95–110.
80 H. C. Schniepp, J.-L. Li, M. J. McAllister, H. Sai, M. Herrera-Alonso, D. H. Adamson, R. K. Prud'homme, R. Car, D. A. Saville and I. A. Aksay, *J. Phys. Chem. B*, 2006, **110**, 8535–8539.
81 V. Gupta, N. Chaudhary, R. Srivastava, G. D. Sharma, R. Bhardwaj and S. Chand, *J. Am. Chem. Soc.*, 2011, **133**, 9960–9963.
82 A. J. Nozik, *Phys. E.*, 2002, **14**, 115–120.
83 A. J. Nozik, *Nano Lett.*, 2010, **10**, 2735–2741.
84 F. Guinea, M. A. H. Vozmediano, M. P. Lopez-Sancho and J. Gonzalez, *Adv. Mater.*, 2011, **23**, 5324–5326.
85 N. Tombros, C. Jozsa, M. Popinciuc, H. T. Jonkman and B. J. van-Wees, *Nature*, 2007, **448**, 571–574.
86 W. Han and R. K. Kawakami, *arXiv*, 2010, **1012**, 3435–3435.
87 A. H. Castro-Neto and F. Guinea, *Phys. Rev. Lett.*, 2009, **103**, 026804–026807.
88 D. Huertas-Herrero, F. Guinea and A. Brataas, *Phys. Rev. Lett.*, 2009, **103**, 146801–146804.
89 F. Guinea, *New J. Phys.*, 2010, **12**, 083063–083071.
90 J. Viana-Gomes, V. M. Pereira and N. M. R. Peres, *Phys. Rev. B: Condens. Matter Mater. Phys.*, 2009, **80**, 245436–245446.
91 J. Guttinger, C. Stampfer, T. Frey, T. Ihn and K. Ensslin, *Phys. Status Solidi B*, 2009, **246**, 2553–2557.
92 M. Sepioni, R. R. Nair, S. Rablen, J. Narayanan, F. Tuna, R. Winpenny, A. K. Geim and I. V. Grigorieva, *Phys. Rev. Lett.*, 2010, **105**, 207205–207208.

93 A. D. Güçlü, P. Potasz, O. Voznyy, M. Korkusinski and P. Hawrylak, *Phys. Rev. Lett.*, 2009, **103**, 246805–246808.
94 X. H. Gao, L. L. Yang, J. A. Petros, F. F. Marshal, J. W. Simons and S. M. Nie, *Curr. Opin. Biotechnol.*, 2005, **16**, 63–72.
95 R. Hardman, *Environ. Health Perspect.*, 2006, **114**, 165–172.
96 Y. Jing, Y. Zhu, X. Yang, J. Shen and C. Li, *Langmuir*, 2011, **27**, 1175–1180.
97 N. W. S. Kam, Z. A. Liu and H. J. Dai, *Angew. Chem., Int. Ed.*, 2006, **45**, 577–581.
98 J. Zhao, G. Chen, L. Zhu and G. Li, *Electrochem. Commun.*, 2011, **13**, 31–33.
99 Y. Li, Y. Zhao, H. Cheng, Y. Hu, G. Shi, L. Dai and L. Qu, *J. Am. Chem. Soc.*, 2012, **134**, 15–18.
100 K. P. Gong, F. Du, Z. H. Xia, M. Durstock and L. M. Dai, *Science*, 2009, **323**, 760–764.
101 R. L. Liu, D. Q. Wu, X. L. Feng and K. Mullen, *Angew. Chem., Int. Ed.*, 2010, **49**, 2565–2569.
102 Z.-J. Zhou, Z.-B. Liu, Z.-R. Li, X.-R. Huang and C.-C. Sun, *J. Phys. Chem. C*, 2011, **115**, 16282–16286.
103 K. Ray, R. Badugu and J. R. Lakowicz, *J. Am. Chem. Soc.*, 2006, **128**, 8998–8999.
104 C. Li, Y. Zhu, X. Zhang, X. Yang and C. Li, *RSC Adv.*, 2012, **2**, 1765.
105 J. Yang, F. Zhang, Y. Chen, S. Qian, P. Hu, W. Li, Y. Deng, Y. Fang, L. Han, M. Luqman and D. Zhao, *Chem. Commun.*, 2011, **47**, 11618–11620.
106 W. Li, D. Portehault, R. Dimova and M. Antonietti, *J. Am. Chem. Soc.*, 2011, **133**, 7121–7127.
107 K.-Y. Niu, H.-M. Zheng, Z.-Q. Li, J. Yang and X.-W. Du, *Angew. Chem., Int. Ed.*, 2011, **50**, 4099–4102.
108 T. M. Atkins, A. Thibert, D. S. Larsen, S. Dey, N. D. Browning and S. M. Kauzlarich, *J. Am. Chem. Soc.*, 2011, **133**, 20664–20667.
109 M. L. Mastronardi, F. Hennrich, E. J. Henderson, F. Maier-Flaig, C. Blum, J. Reichenbach, U. Lemmer, C. Kubel, D. Wang, M. M. Kappes and G. A. Ozin, *J. Am. Chem. Soc.*, 2011, **133**, 11928–11931.
110 Y. He, Y. Zhong, F. Peng, X. Wei, Y. Su, Y. Lu, S. Su, W. Gu, L. Liao and S.-L. Lee, *J. Am. Chem. Soc.*, 2011, **133**, 14192–14195.